A modeling study of temporal and spatial pCO$_2$ variability on the biologically active and temperature-dominated Scotian Shelf

Krysten Rutherford[1], Katja Fennel[1], Dariia Atamanchuk[1], Douglas Wallace[1], Helmuth Thomas[1,2]

[1]Department of Oceanography, Dalhousie University, 1355 Oxford Street, Halifax, Nova Scotia, B3H 4R2, Canada
5 [2]Institute of Coastal Research, Helmholtz Center Geesthacht, D-215502 Geesthacht, Germany

Correspondence to: Krysten Rutherford (krysten.rutherford@dal.ca)

Abstract. Continental shelves are thought to be affected disproportionately by climate change and are a large contributor to global air-sea carbon dioxide (CO$_2$) fluxes. It is often reported that low-latitude shelves tend to act as net sources of CO$_2$ whereas mid- and high-latitude shelves act as net sinks. Here, we combine a high-resolution regional model with surface water
10 time-series and repeat transect observations from the Scotian Shelf, a mid-latitude region in the northwest North Atlantic, to determine what processes are driving the temporal and spatial variability of partial pressure of CO$_2$ (pCO$_2$). In contrast to the global trend, the Scotian Shelf acts as a net source. Surface pCO$_2$ undergoes a strong seasonal cycle associated with both a strong biological drawdown of Dissolved Inorganic Carbon (DIC) in spring, and pronounced effects of temperature, which ranges from 0°C in the winter to near 20°C in the summer. Throughout the summer, events with low surface-water pCO$_2$ occur
15 nearshore associated with coastal upwelling. This effect of upwelling on pCO$_2$ is also in contrast to the general assumption that upwelling increases surface pCO$_2$ by delivering DIC-enriched water to the surface. Aside from these localized events, pCO$_2$ is relatively uniform across the shelf. Our model agrees with regional observations, reproduces seasonal patterns of pCO$_2$, and simulates annual outgassing of CO$_2$ from the ocean of +1.9 ± 0.2 mol C m^{-2} yr^{-1} for the Scotian Shelf, net neutral CO$_2$ flux of -0.09 ± 0.16 mol C m^{-2} yr^{-1} for the Gulf of Maine and uptake by the ocean of -0.88 ± 0.4 mol C m^{-2} yr^{-1} for the
20 Grand Banks.

1 Introduction

The global ocean acts as a major sink of CO$_2$ from the atmosphere (e.g., Le Quéré et al 2018; Gruber et al. 2019; Landschützer et al. 2014; Rodenbeck et al. 2015), but it has been suggested that flux density (or flux per unit area) on continental shelves is larger than in the open ocean (Chen et al. 2013; Laruelle et al. 2014). Therefore, compared to their size, continental shelves
25 are thought to disproportionately contribute to global air-sea CO$_2$ fluxes (Laruelle et al. 2010). Additionally, they are susceptible to climate change on much shorter timescales than the open ocean (Cai et al. 2010) and are experiencing increasing impacts of human activity (Cai 2011; Doney 2010; Gruber 2015). Given their high susceptibility to negative impacts from climate change, and their potentially significant contribution to global air-sea CO$_2$ fluxes, it is important to understand the drivers underlying inorganic carbon dynamics on continental shelves.

30   It is generally thought that continental shelves at mid to high latitudes act as net sinks of atmospheric CO_2 while those at low latitudes act as net sources (e.g. Chen & Borges 2009; Cai et al. 2006; Laruelle et al. 2014; Roobaert et al. 2019). There are, however, notable deviations from this global-scale pattern. The Scotian Shelf, a mid-latitude shelf off the coast of eastern Canada, is one example with large discrepancies between independent estimates of air-sea CO_2 flux (Fennel et al. 2019). Direct measurements made using a moored CARIOCA buoy on the Scotian Shelf indicate that the shelf acts as a net source of CO_2

35   to the atmosphere (Shadwick et al. 2010; Shadwick et al. 2011; Shadwick & Thomas 2014). These findings are in contrast to other observation-based studies indicating that the Scotian Shelf follows the global trend and acts as a net sink of CO_2 (Laruelle et al. 2014; Laruelle et al. 2015; Signorini et al. 2013). These contrasting results for the Scotian Shelf emphasize the large uncertainty inherent in shelf-wide CO_2 flux estimates.

       Continental shelves are highly complex and dynamic regions where many biological and physical processes modulate

40   CO_2 flux (Laruelle et al. 2014; Laruelle et al. 2017; Roobaert et al. 2019). The partial pressure of CO_2 (pCO$_2$) in the ocean is one of the key factors which determines the air-sea CO_2 flux. Recent global studies found that thermal controls dominate the seasonality of pCO$_2$ but that these alone cannot describe observed pCO$_2$ variations, particularly in temperate and high latitudes (Roobaert et al. 2019). High rates of primary production on continental shelves (Chen & Borges 2009) are another important driver of seasonal changes in pCO$_2$.

45   Continental margins are also subject to intense horizontal transport processes, which act as additional drivers of CO_2 fluxes. For example, the Continental Shelf Pump, a term first coined by Tsunogai et al. (1999) in relation to the East China Sea, describes the movement of shelf water high in dissolved inorganic carbon (DIC) across the shelfbreak to the subsurface open ocean leading to an influx of atmospheric CO_2. This mechanism is thought to mainly occur at mid- to high-latitude shelves since it relies on winter cooling to create dense shelf water that is transported to the open ocean's subsurface layers.

50   Upwelling is another well-studied transport mechanism driving shelf-wide CO_2 dynamics. The California Current system is a typical example of an upwelling system (Chavez et al. 2017; Hickey 1998; Fennel et al. 2019). Here, winds drive coastal upwelling, which brings DIC-rich water to the surface along the continental shelf and creates favourable conditions for CO_2 outgassing to the atmosphere.

       Altogether, these complex shelf dynamics lead to large spatial and temporal variability of pCO$_2$ (Previdi et al. 2009).

55   Such large variability combined with limited data availability for many continental shelves make it difficult to accurately constrain CO_2 fluxes. Limited data availability in space and time, often with seasonal biases, is a prime source of uncertainty in flux estimates that can only be overcome with more uniformly distributed sampling. To fully capture how ocean margins are reacting to perturbations caused by the steady input of anthropogenic CO_2 to the atmosphere, it is important to understand the processes underlying both spatial and temporal evolution of shelf-wide pCO$_2$.

60   Numerical models can be useful when investigating such complex interactions and constraining CO_2 flux since they can interpret sparse measurements through the mechanistic representations of relevant processes. In the present study, we employ a high-resolution biogeochemical model of the northwest North Atlantic to examine the magnitude, variability and sign of the air-sea CO_2 flux on the Scotian Shelf. Previous studies have shown that our model accurately represents the physical

(Brennan et al. 2016, Rutherford & Fennel 2018) and biological (Laurent et al. 2020) dynamics of the region. Here, we focus
65   solely on the model representation of inorganic carbon dynamics, especially the spatial and temporal variability of $p\mathrm{CO_2}$ on
the Scotian Shelf in light of new, high-resolution, shelf-wide observations.

      Our overall goal is to show how both biological and transport processes work together on the Scotian Shelf to set
shelf-wide surface $p\mathrm{CO_2}$. We additionally emphasize event-based variability of the air-sea $\mathrm{CO_2}$ flux, and, especially, how
short-term, upwelling-favourable wind events throughout the summer create spatial variability of $\mathrm{CO_2}$ on the Scotian Shelf.
70   To accomplish these goals, our paper: (1) discusses the seasonality of $p\mathrm{CO_2}$ across the shelf; (2) investigates the spatial
variability of $p\mathrm{CO_2}$, particularly during the summer months and (3) reports shelf-wide air-sea $\mathrm{CO_2}$ flux estimates in comparison
to previously reported estimates. We discuss the importance of our findings in terms of global patterns of air-sea $\mathrm{CO_2}$ flux and
carbon cycling.

2 Study Region

75   The Scotian Shelf (Figure 1) is uniquely located at the junction of the subpolar and subtropical gyres (Loder et al. 1997; Hannah
et al. 2001). Regional circulation is dominated by southward transport of the Labrador Current (Loder et al. 1998; Fratantoni
& Pickart 2007). As a result, cool Arctic-derived water accumulates along the northwestern North Atlantic continental shelf
separating fresh shelf waters from warmer and salty slope waters (Beardsley & Boicourt 1981; Loder et al. 1998; Fratantoni
& Pickart 2007).

80   The Scotian Shelf in particular is controlled by inshore and shelf-break branches of the southwestward moving
current. The shelf-break branch inhibits the movement of water across the shelf break of the Scotian Shelf (Rutherford &
Fennel 2018). As a result, water moves predominantly along-shelf so that residence times in the region are relatively long,
with water being retained on the Scotian Shelf for an average of 3 months before moving further southwest on the shelf
(Rutherford & Fennel 2018). In terms of vertical structure, the Scotian Shelf shifts between a two-layer system in the winter,
85   when a cold, fresh layer sits over a warm, salty deep layer, and a three-layer system in the spring and summer, when a warm
surface layer forms in the top 20 m above the cold intermediate layer between 20 – 100 m, and the warm and salty deep layer
(Dever et al. 2016).

      The Scotian Shelf is additionally characterized by a large, shelf-wide spring bloom initiated in late-March (Ross et
al. 2017; Fournier et al. 1977; Mills & Fournier 1979), when the mixed layer is still relatively deep and temperature is at its
90   coldest (Craig et al. 2015). The initiation of the spring bloom in late-March has rapid and large impacts on the observed $p\mathrm{CO_2}$
seasonality (Shadwick et al. 2010; Shadwick et al. 2011).

3 Methods

3.1 Model setup & initialization

3.1.1 Physical Model Setup

95   We employ a biogeochemical model, based on Fennel et al. (2006), Fennel & Wilkin (2009) and Laurent et al. (2020) that is part of the Regional Ocean Modelling System (ROMS, v.3.5; Haidvogel et al. 2008). The physical model implementation, described in more detail in Brennan et al. (2016), has 30 vertical levels and approximately 10-km horizontal resolution (240x120 horizontal grid cells), uses the GLS vertical mixing scheme (Umlauf & Burchard 2003; Warner et al. 2005), atmospheric surface forcing from the European Centre for Medium-Range Weather Forecasts (ECMWF) global atmospheric

100   reanalysis (Dee et al. 2011) and the "*h*igh-order *s*patial *i*nterpolation at the *m*iddle *t*emporal level" (HSIMT) advection scheme for tracers (Wu & Zhu 2010). Physical initial and boundary conditions are defined using the regional physical ocean model of the northwest North Atlantic of Urrego-Blanco & Sheng (2012). Temperature and salinity are nudged toward the climatology of Geshelin et al. (1999) in a 10-grid-cell wide buffer zone along open boundaries. Nudging strength decays linearly away from the boundaries to a value of zero in the 11th grid cell from the boundary. Tides are imposed from Egbert & Erofeeva

105   (2002). Climatological river discharge is imposed for 12 major rivers and uses observed long-term monthly means from Water Survey Canada. Full details on the physical model setup and its validation can be found in Brennan et al. (2016) and Rutherford & Fennel (2018).

3.1.2 Biogeochemical Module

The biogeochemical model is based on the nitrogen-cycle model with inorganic carbon component of Fennel et al. (2006) and

110   Fennel & Wilkin (2009) but was recently expanded to include 2 phytoplankton and 2 zooplankton functional groups (Laurent et al. 2020). For a detailed description and validation of the biological model, we refer to Laurent et al. (2020), who also showed that it outperforms global models for the region in terms of model skill.

      For calculating air-sea CO_2 flux, according to the carbonate chemistry model of Zeebe & Wolf-Gladrow (2001), we use dissociation constants (K1 and K2) from Millero et al. (1995) using Mehrbach et al. (1973) data on the seawater scale.

115   Atmospheric pCO$_2$ is set to the seasonal cycle and secular trend derived from Sable Island monitoring data contributed by Environment Canada's Greenhouse Gas Measurement Program (Environment and Climate Change Canada, 2017). CO_2 solubility is calculated with the Weiss (1974) formulation. The gas transfer coefficient of Ho et al. (2006) is used and depends on wind speed at 10 m above the sea surface and the Schmidt number. Further details of the biogeochemical model, including the carbonate chemistry equations, can be found in Laurent et al. (2017, Supporting Information). Carbon initialization,

120   boundary conditions and climatological nudging are calculated from relationships with temperature and salinity determined from bottle data for the region. DIC is nudged in an 80-grid-cell wide buffer zone along the eastern boundary, with nudging linearly decaying away from the boundary to a value of 0 in the 81st grid cell. At all other boundaries, a 10-grid buffer zone is

used, as with temperature and salinity. The buffer zone is wider in the eastern boundary to eliminate a numerical drift in DIC at the northeastern boundary.

125   Nitrate concentrations in rivers are prescribed from Global NEWS model output Seitzinger et al. (2005). DIC and total alkalinity (TA) in rivers were calculated by fitting a linear relationship with salinity from Gulf of St. Lawrence bottle data and extrapolating to river water salinity. The model is initialized on January 1, 1999 from Urrego-Blano and Sheng's (2012) solution for physics, dissolved oxygen (O_2) and nitrate (NO_3^-) concentrations are initialized from the regional climatologies (Kuhn 2017; Laurent et al. 2020), and DIC and TA are initialized from observationally based relationships with temperature

130   (T) and salinity (S) using data from December, January and February ($TA = 43S + 800$, $r^2 = 0.92$; $DIC = 1153 - 21.6T + 29.1S - 0.41T^2 + 0.63ST$, $r^2 = 0.90$). The model is run for 6 years (1999-2004) with daily output and the first year is discarded as spin-up.

3.2 Observational Datasets

The moored CARIOCA buoy was located at Station 2 on the Halifax Line. Station 2 (HL2; 44.3°N, 63.3°W) is located about

135   30 km offshore from Halifax, Nova Scotia, and occupied monthly by Bedford Institute of Oceanography. The buoy measured surface water (at approximately 1 m depth) temperature, conductivity, pCO_2, salinity and Chl-a fluorescence every hour and was deployed from 2007 to 2014 with several gaps in data due to calibration and maintenance (see Table S1 in Supplement). pCO_2 was estimated using an automated spectrophotometric technique (Lemay et al. 2018). The raw pCO_2 data contained high-amplitude spikes, with increases from 400 µatm to over 1000 µatm within a few hours, which were measuring artifacts

140   and did not represent $pCO2$ of surrounding water. These spikes were removed by binning all years of the pCO_2 observations into a 365-day of year (DOY) seasonal cycle. Any points that were outside 1.5 standard deviations of the 1-month moving average pCO_2 where discarded. This method removed only the extreme values and maintained much of the observed variability (see Figure 2).

       The sensor-based underway system, Dal-SOOP (Arruda et al., 2020), was installed on the multipurpose platform

145   supply vessel Atlantic Condor (operated by Atlantic Towing Ltd.) and has been measuring a suite of biogeochemical parameters, including pCO_2, in the surface water since May 2017. The ship transits weekly to biweekly between the Halifax and the Deep Panuke gas platform off Sable Island on the Scotian Shelf (Figure 1). The Atlantic Condor pCO_2 data underwent standard QA/QC procedures, which included pre-, post-deployment and regular zero-calibration of the pCO_2 sensor (Pro-Oceanus Inc, Canada) and associated data corrections. The QC'd data has been deposited into the Surface Ocean CO_2 Atlas

150   (SOCAT v.2020), where it was attributed an accuracy of ±10 µatm. Performance of the novel Dal-SOOP system was assessed during a 2-month transatlantic cruise in comparison with a conventional pCO_2 equilibrator and showed good agreement with the latter (i.e. −5.7 ± 4.0 µatm; Arruda et al., 2020).

       During the QC/QA procedure, some data collected in close proximity to Halifax, and corresponding to the outbound transects, were removed. Some of these data were biased high and attributed to prolonged ship layover in port allowing for a

155   build-up of high pCO_2 within the Dal-SOOP system due to respiration. The active pumping that delivers fresh seawater to the

measurement system is triggered by a GPS signal when the ship leaves the harbour; as a result, there can be a delayed response from the pCO_2 sensor to the much lower pCO_2 signals observed immediately outside the harbour. To account for the bias, values that were 2 standard deviations from the mean pCO_2 value for the latitudinal bin closest to the Halifax Harbour were removed for some transects. Only three transects were removed.

4 Results

4.1 CO₂ Timeseries and Transect

Both the model and observations at the CARIOCA buoy location (see Figure 1) are shown as a seasonal cycle in Figure 2 (from top to bottom: chlorophyll, pCO_2, temperature and temperature normalized pCO_2). The buoy observations show a distinct and recurring seasonal cycle in pCO_2. Specifically, pCO_2 is relatively constant (~ 425 µtm) from day 0 to 75. In late March, at approximately day 75, there is a large (100-200 µatm) and rapid (over ~ 25 days) drop of pCO_2 associated with DIC drawdown due to the spring bloom (the dashed line indicates the peak in chlorophyll and its alignment with the lowest pCO_2 value). This drawdown of DIC occurs while the surface temperature is relatively constant and at its annual minimum.

Following the drop in pCO_2 associated with the spring bloom, around day 100, surface water starts to warm, and this warming dominates the pCO_2 seasonal cycle with a maximum value of approximately 450–500 µatm reached around day 200-250 (mid to late summer). Around day 250, temperatures and pCO_2 start to decrease. Also shown is the temperature-normalized pCO_2 using the Takahashi et al. (2002) method for removing the thermal component of pCO_2 variations. The biological drawdown of DIC is visible in the temperature-normalized pCO_2 during the spring bloom starting around day 75 and a further decline throughout summer from day 150 to 250. This indicates that the overall increase in the non-normalized pCO_2 in summer is driven by increasing temperatures, and that biological process tend to draw down DIC during this period.

Most of the Atlantic Condor observations at this location fall within the envelope of the buoy observations' pCO_2 seasonal cycle. The monthly mean SOCAT v2020 pCO_2 for the entire Scotian Shelf also fall within the spread of buoy observations for most months. Exceptions include February and August when the SOCAT observations are lower than the buoy observations, and September and October when the SOCAT observations are at the low end of the observations.

In terms of quantitative metrics, the model at the buoy location has an overall bias of -21.3 µatm and RMSE of 58.1 µatm compared to the buoy data. The model underestimates pCO_2 throughout January and February (day 0 - 80) partly because its spring bloom starts earlier than in the observations. The bloom-related minimum in pCO_2 in the model is approximately 50-75 µatm higher than the buoy observations but is consistent with the Atlantic Condor observations. Temperature then dominates the pCO_2 seasonality in the model over a similar period as in the observations. During the summer (day 150-300), the model slightly overestimates pCO_2 but follows a similar cycle as the observations throughout the remainder of the year. The temperature-normalized pCO_2 has similar biases (underestimation from day 0-80; overestimation from day 150-300), an RMSE of 63.6 µatm and an overall bias of -29.5 µatm.

A comparison of simulated pCO_2 with the Atlantic Condor Transect observations along the average ship track (Figure 1) is shown in Figure 3. Compared to the Atlantic Condor observations, the model has a bias of 4.1 µatm and an RMSE of 20.3 µatm. The bias is about half in magnitude as that at the buoy and positive, indicating that the model tends to slightly

190 higher pCO_2 across the shelf than the ship data. The seasonal cycle along the ship track (Figure 3) is similar to that at the buoy (Figure 2). The top panel of Figure 3 shows qualitatively good agreement between the model and observations across the whole transect, which is reflected in the averaged pCO_2 in the bottom panel. The model does a very good job at representing pCO_2 throughout the winter (November through March) but does not reproduce the full spring bloom drop in pCO_2 across the whole shelf throughout April as observed. The model also overestimates pCO_2 throughout most of June and July. The seasonal cycle

195 across the transect is relatively uniform throughout most of the year; however, there are some exceptions, for example, throughout July pCO_2 is relatively low nearshore in both the model and observations. There are also a couple of transects in 2019, not seen in any of the other years, where observations show high pCO_2 values nearshore (June, July and November of 2019). These are thought to be artifacts of the sampling system resulting from remnant respiration signals from Halifax harbour.

4.2 Effects of Upwelling Events

200 To better understand the effect of physical events on shelf-wide pCO_2, this section focuses on the cross-shelf variations in year 2000. Figure 4 shows the evolution of pCO_2 along the Atlantic Condor transect throughout the year in both model (Figure 4a) and observations (Figure 4b). As in Figure 2 and Figure 3, the seasonal cycle of pCO_2 extends across the entire shelf. Starting in January (light beige), pCO_2 is around 400 µatm. In March (~ day 50; golden orange colour), pCO_2 starts to decrease, reaching a minimum of approximately 325 µatm in the model and around 275-300 µatm in the observations (day 100; dark brown

205 colour). pCO_2 subsequently increases again due to warming in the late-spring/early-summer and reaches a maximum of about 550 µatm in the model and 525 µatm in the observations (day 200; purple values). Following this peak in pCO_2, both the model and observations start to decline, associated with cooling (days 225 to 325; purple to light blue).

The insets in Figure 4 highlight events in summer (purple), in the northwestern half of the transect closest to Halifax, when pCO_2 decreases by 50 – 100 µatm within 40-80 km off the coast in the model and approximately 25 km off the coast in

210 the observations. These events are also visible in Figure 5, which shows the pCO_2 seasonal cycle (top panel) in two longitudinal bins along the Atlantic Condor transect. The bin locations are shown in Figure 1 and contrast data closest to the coastline (-63.5 to -63; blue) with data closest to the shelf break (-61 to -60.5; pink) for both the model (lines) and observations (points). There is good agreement between the model and observations in terms of seasonality and the along-transect differences in pCO_2. Throughout most of the year, pCO_2 is relatively uniform across the shelf, with a tendency towards slightly higher pCO_2

215 nearshore versus offshore (see panels b and d). However, throughout the summer months (days 150 – 250) there are events in both the model and observations where pCO_2 is much lower along the coastline of Nova Scotia (blue) in comparison to near the shelf break (pink). Panels c and f illustrate how these low pCO_2 events correspond to low temperature events nearshore. During some of these events, temperature nearshore is about 7°C lower than near the shelf break.

The top panel in Figure 6 shows a snapshot of surface pCO_2 from the model during one of the upwelling events (thick black line in Figure 5a). pCO_2 is relatively uniform across most of the shelf. However, in a narrow band along the coastline, pCO_2 values are 50 – 100 µatm lower than the rest of the shelf. The bottom two panels in Figure 6 shows transects of temperature (middle panel) and DIC (bottom panel) with density contours along the Atlantic Condor transect for the same time slice. In both the middle and bottom panels, the density gradients move upwards towards the coastline, consistent with upwelling events. This upwelling brings cooler temperatures and higher DIC concentrations to the surface along the coastline of Nova Scotia. The low pCO_2 bin ranges from -63.5 to – 63° longitude in the model (approximately -63.5 to – 63.3° longitude in the observations; Figure 4), and aligns with the surface area affected by the upwelling events (Figure 6) in the model.

The effect of upwelling-favourable wind on pCO_2 and air-sea CO_2 flux at different locations on the shelf (bins 1 and 2, Figure 1) throughout summer 2000 are shown in Figure 7. The top panel illustrates the alignment of upwelling-favourable winds with the low pCO_2 events nearshore. These upwelling events and the subsequent low pCO_2 signal result in lower air-sea CO_2 fluxes nearshore (blue) compared to farther offshore (pink) throughout the summer (at approximately half the flux value nearshore versus offshore throughout July).

4.3 Regional Flux Estimates

The model-simulated air-sea CO_2 fluxes, integrated by month and year, for the Scotian Shelf and at the buoy location are shown in Figure 8 in comparison to the flux calculated from the CARIOCA buoy observations. Annually, the averaged flux between the model and observations is comparable, and the flux estimates at the buoy location are significantly larger than the shelf-wide flux estimates. The uncertainty in the model estimates is calculated as the standard deviation between years. The model-estimated, annually integrated flux for the Scotian Shelf shows outgassing of CO_2 at $+1.9 \pm 0.2$ mmol C m^{-2} yr^{-1}. At the buoy location, the model estimates net outgassing of $+2.4 \pm 0.2$ mmol C m^{-2} yr^{-1}. From the buoy observations, the annually integrated CO_2 flux is estimated as net outgassing at $+1.5 \pm 1.4$ mmol C m^{-2} yr^{-1}. Although our model-derived estimate is within the upper error-bound of the observation-based estimate, it is slightly higher which may be due to the model's slight overestimation of pCO_2, particularly throughout the summer months. There are also some differences on the seasonal scale. In the model, the Scotian Shelf flux is lower in magnitude than the flux at the buoy location during most of the year, and particularly from June to January. Additionally, the observational CO_2 flux from the buoy measurements is only higher in magnitude than the model-based flux during the spring bloom.

Figure 9 compares the model-derived, annual flux estimates from the present study for the Scotian Shelf ($+1.9 \pm 0.2$ mmol C m^{-2} yr^{-1}), Grand Banks (-0.88 ± 0.4 mol C m^{-2} yr^{-1}) and Gulf of Maine (-0.09 ± 0.16 mol C m^{-2} yr^{-1}) to previously reported estimates. The model estimate for the Scotian Shelf agrees well with the estimates from Shadwick et al. (2011) but disagrees with those from Signorini et al. (2013), Laruelle et al. (2014) and Laruelle et al. (2015). Laruelle et al. (2014) define the shelf region as a larger area that encompasses both the Scotian Shelf and Gulf of Maine. Laruelle et al. (2015) calculate one flux estimate for both the Scotian Shelf and Gulf of Maine. Signorini et al. (2013) calculates separate estimates for Gulf

of Maine and Scotian Shelf. The model estimate for the Gulf of Maine falls within all of the estimates for the region and agrees best with the estimates from Signorini et al. (2013).

5 Discussion

We have compared the inorganic carbon dynamics in our medium complexity biogeochemical model of the northwest North
255 Atlantic against two different observational datasets of pCO$_2$, one of them highly resolved in time from a CARIOCA buoy and the other with high spatial resolution along a cross-shelf transect that is occupied approximately bi-weekly. The largest limitation of the model is that it is unable to capture the speed and magnitude of the DIC drawdown associated with the spring bloom throughout March and April (Figure 2 and Figure 3). The simulated pCO$_2$ starts to decline earlier and over a longer period than in both the buoy and transect observations, and the transect shows that this timing is consistent across the whole
260 shelf. Additionally, the model does not reach the observed pCO$_2$ minimum during the bloom across the whole shelf. This discrepancy appears to be a result of the bloom initiation occurring slightly too early and the bloom spanning a longer period of time in the model, and also because chlorophyll levels in the model do not reach the peak values that are observed (Figure 2a). This limitation aside, the overall seasonal cycle and switch between biological- and temperature-dominated signals in pCO$_2$ are accurately captured and the model simulates both the spatial and temporal variability of pCO$_2$ across the Scotian
265 Shelf reasonably well.

Coastal upwelling events are major drivers of spatial variability of pCO$_2$ on the Scotian Shelf throughout the summer months. The physical dynamics of coastal upwelling is well-documented on the Scotian Shelf (Petrie et al. 1987; Shan et al. 2016). This upwelling only affects the nearshore region (within ~ 25 km of shore in the observations; within 40-80 km of shore in the model) where water from the deep basins and the cold intermediate layer are transported to the surface. In the model,
270 this creates a coastal band of cold water at the surface that is high in DIC and low in pCO$_2$ (Figure 6). The difference between inshore and offshore temperatures (8°C and 15°C, respectively) during these events has a larger influence on the pCO$_2$ spatial variability than the DIC variations (2060 mmol C m^{-3} inshore and 2020 mmol C m^{-3} offshore; Figure 6) because the thermodynamic influence of temperature outweighs the effect of a slight increase in DIC, thus lowering pCO$_2$. This is contrary to the generally assumed and expected effect of coastal upwelling on pCO$_2$. For the given range of DIC values (2060 to 2020
275 mmol C m^{-3}) and a mean temperature of 11°C, the thermodynamic effect outweighs the effect of DIC differences for temperature changes larger than 4°C. Typically, it is thought that upwelling of subsurface waters rich in DIC leads to increased surface pCO$_2$ as is the case for the California Current System, encompassing the continental shelves off of Washington, Oregon and California, where nearshore outgassing of CO$_2$ during upwelling events is well documented (Fennel et al. 2019, Chavez et al. 2017, Evans et al. 2015, Fiechter et al. 2014, Turi et al. 2014). In the present study, upwelling events dominate the CO$_2$
280 signal in the summer on the inner portion of the shelf, and act to lower pCO$_2$ and lead to reduced outgassing compared to the rest of the shelf.

Throughout the remainder of the year, the pCO_2 distribution across the Scotian Shelf is relatively uniform (Figure 3). Comparison of the inner and outer shelf pCO_2 (Figure 5) shows the similar seasonality that is seen across the shelf, both in the model results and Atlantic Condor observations. Overall, the location of the CARIOCA buoy is fairly representative of the shelf-wide pCO_2 dynamics.

According to the model, the Scotian Shelf acts as a net source of CO_2 to the atmosphere ($+1.9 \pm 0.2$ mol C m^{-2} yr^{-1}), the Gulf of Maine is neutral (-0.09 ± 0.16 mol C m^{-2} yr^{-1}) and the Grand Banks act as a net sink of CO_2 (-0.88 ± 0.4 mol C m^{-2} yr^{-1}). These results are in agreement with Shadwick et al. (2014) for the Scotian Shelf and Signorni et al. (2013) for the Gulf of Maine. Our results disagree, however, with results from other global (Laruelle et al. 2014) and regional studies (Laruelle et al. 2015; Signorini et al. 2013). The discrepancy in reported air-sea CO_2 flux between these studies is partly a result of how each study defines the area of the Scotian Shelf and Gulf of Maine. For example, Laruelle et al. (2015) calculates one estimate for both the Scotian Shelf and Gulf of Maine. The shelves of eastern North America are diverse, particularly in width and circulation features, and defining them as a single region is not representative. Additionally, the Scotian Shelf waters are strongly influenced by cold, carbon-rich Labrador Sea water, which is not the dominant endmember south of the Gulf of Maine (Loder et al. 1998, Rutherford & Fennel 2018; Fennel et al. 2019). Calculating a single flux estimate for the entirety of this dynamically diverse region is problematic and will yield a different estimate than when considering smaller and more specific regions. However, this only partially explains the difference in flux estimates.

Another reason is that the global SOCAT database was missing important regional data until recently. Signorini et al. (2013) used data from version 1.5 and Laruelle et al. (2014, 2015) used data from version 2.0 of the SOCAT database. Neither of the observational datasets used in the present study were included in SOCAT versions 1.5 and 2.0. Figure 10 illustrates the difference between different SOCAT versions for seasonal pCO_2 on the Scotian Shelf. SOCAT v2020 has consistently higher average pCO_2 values than v1.5 and v2, with at least double the number of years and a much larger number of observations going into each monthly average (on the order of 1000 to 10000 measurements in v2020 versus 100 to 1000 in v1.5 and v2). We believe that flux estimates using the updated SOCAT v2020 will agree better with our estimates and those of Shadwick et al. (2014).

In the present study, we have synthesized and compared our model simulations with high-resolution observations to highlight the dependence of Scotian Shelf pCO_2 seasonality on: (1) biological drawdown of DIC during the spring bloom, (2) temperature effects throughout the summer months, and (3) wind-driven coastal upwelling events. In Figure 2d, the temperature-normalized pCO_2 shows the non-thermal pCO_2 signal, which distinguishes the influence of biological and transport processes on pCO_2 (Takahashi et al. 2002). There is a clear decrease of pCO_2 associated with the spring bloom. The simulated decrease in pCO_2 is smaller than in the observations, likely due to the bloom occurring too early and over a more extended period in the model than the observations. In summer, temperature-normalized pCO_2 continues to decrease rather than follow the increasing temperature signal of non-normalized pCO_2. This agrees with the findings of Shadwick & Thomas (2014) that, in summer, the thermodynamic signal in pCO_2 outweighs the influence of biological activity. We believe this

315 thermodynamic influence is an important factor driving the net outgassing observed on the Scotian Shelf, particularly when combined with the delivery of DIC-rich water from the Labrador Sea.

Understanding what processes presently control CO_2 dynamics is important for projecting how the region will be affected by changes in climate. Previous studies have suggested that the frequency and intensity of coastal upwelling could increase (e.g., Xiu et al. 2018). In the case of the Scotian Shelf, increased upwelling would lead to less outgassing or even net
320 ingassing during summer along the coast of Nova Scotia. Climate change could therefore disproportionately affect the nearshore region here and lead to an intensification of spatial gradients. Such an upwelling signal would be in addition to the effect of increasing atmospheric CO_2, which may be driving the entire Scotian Shelf towards a more neutral system with less outgassing. The effect of the thermal control on Scotian Shelf pCO_2 is also an important aspect to consider. As temperatures continue to rise, summer pCO_2 values will also likely increase, potentially offsetting some of the effect of increased
325 atmospheric CO_2 but also affecting production and respiration rates. Of course, none of these factors act independently and will instead combine to alter both the seasonal and spatial patterns of pCO_2 in the region, making the overall outcome of climate-related perturbations on the Scotian Shelf difficult to predict. However, the implementation of a regional model that resolves current conditions well, as in the present study, is an important step towards projecting future climate-related changes in the region.

330 **6 Conclusions**

In this study, we have validated surface pCO_2 fields from a medium-complexity regional biogeochemical model for the northwest North Atlantic shelf region against pCO_2 observations from a CARIOCA buoy and repeated cross-shelf transects from a ship of opportunity that crosses the Scotian Shelf. Except for the strength and speed of the pCO_2 drawdown associated with the spring bloom, the model simulations represent the observed spatial and temporal variability of pCO_2 on the Scotian
335 Shelf well. Contrary to most coastal upwelling systems, upwelling events in summer are acting to lower pCO_2 within ~25 km of the coastline, as cold, carbon-enriched water is brought to the surface. The lowering of surface pCO_2 during these events occurs because the temperature effect leading to a lowering of pCO_2 overwhelms the increase in pCO_2 associated with DIC enrichment. We found pCO_2 to be relatively uniform across the shelf, with the exception of a narrow band near shore impacted by summer upwelling events. Overall, the Scotian Shelf acts as a net source of CO_2 ($+1.9 \pm 0.2$ mol C m^{-2} yr^{-1}), the Gulf of
340 Maine is net neutral (-0.09 ± 0.16 mol C m^{-2} yr^{-1}) and Grand Banks acts as a net sink of CO_2 (-0.88 ± 0.4 mol C m^{-2} yr^{-1}) in our simulation. Combination of the model simulation and the highly resolved observational data sets emphasizes that the seasonal cycle of pCO_2 is driven by strong biological drawdown of DIC in early spring and a dominant thermal control throughout the summer months. Except for the short spring bloom period, surface pCO_2 is oversaturated with respect to atmospheric values, which results in net outgassing. Ongoing changes in climate and carbon cycling will likely alter both the
345 seasonal and spatial patterns of pCO_2 on the Scotian Shelf, and may disproportionately affect the nearshore region as upwelling events are predicted to increase.

Acknowledgements

We acknowledge funding by the Marine Environmental Observation, Prediction and Response Network (MEOPAR). This work was additionally funded in part by the Canada Excellence Research Chair (CERC) in Ocean Science and Technology at

350 Dalhousie University and Canada Foundation for Innovation (CFI) project number 29011. We would like to thank the captain and crew of Atlantic Condor for their continuing support in operating the Dal-SOOP underway system. Mike Vining, Jeremy Lai, Dan Kehoe, Kitty Kam and Jordan Sawler contributed to the design, installation and maintenance of the underway system. We also are grateful for the use of observational datasets to initialize our model from Kumiko Azetsu-Scott (Department of Fisheries and Oceans Canada) and Alfonso Mucci (McGill University). We would also like to acknowledge the use of the

355 scientific colourmaps lapaz, vikO, and batlow (Crameri 2018) used in this study.

References

Arruda, R., Atamanchuk, D., Cronin, M., Steinhoff, T., and Wallace, D. W.: At-sea intercomparison of three underway pCO_2 systems, Limnology and Oceanography Methods, 18 (2), 63-76, doi:10.1002/lom3.10346, 2020.

Beardsley, R. C. and Boicourt, W. C.: On estuarine and continental shelf circulation in the Middle Atlantic Bight, in: Evolution

360 of Physical Oceanography, pp 198-233, 1981.

Brennan, C. E. , Bianucci, L., and Fennel, K.: Sensitivity of northwest North Atlantic shelf circulation to surface and boundary forcing: A regional model assessment. Atmosphere-Ocean, 54(3), 230-247, doi:10.1080/07055900.2016.1147416, 2016.

Cai., W.-J.: Estuarine and coastal ocean carbon paradox: CO_2 sinks or sites of terrestrial carbon incineration? Annual Review of Marine Science, 3 (1), 123-145, doi:10.1146/annurev-marine-120709-142723, 2011.

365 Cai, W.-J., Chen, L., Chen, B., Gao, Z., Lee, S. H., Chen, J., Pierrot, D., Sullivan, K., Wang, Y., Hu, X., et al.: Decrease in the CO_2 uptake capacity in an ice-free arctic ocean basin. Science, 329(5991), 556-559, doi: 10.1126/science.1189338, 2010.

Cai, W.-J. , Dai, M., and Wang, Y.: Air-sea exchange of carbon dioxide in ocean margins: A province-based synthesis, Geophysical Research Letters, 33(12), doi:10.1029/2006GL026219, 2006.

Chavez, F. P., Pennington, J. T., Michisaki, R. P., Blum, M., Chavez, G. M., Friederich, J., Jones, B., Herlien, R., Kieft, B.,

370 Hobson, B., et al.: Climate variability and change: Response of a coastal ocean ecosystem, Oceanography, 30, 128-145, 2017.

Chen, C.-T. A. and Borges, A. V.: Reconciling opposing views on carbon cycling in the coastal ocean: Continental shelves as sinks and near-shore ecosystems as sources of atmospheric CO_2, Deep Sea Research Part II: Topical Studies in Oceanography, 56(8-10), 578-590, doi:10.1016/j.dsr2.2009.01.001, 2009.

Chen, C.-T. A., Huang, T.-H., Chen, Y.-C., Bai, Y., He, X., and Kang, Y.: Air sea exchanges of CO_2 in the world's coastal

375 seas, Biogeosciences, 10(10), 6509-6544, doi:10.5194/bg-10-6509-2013, 2013.

Craig, S. E., Thomas, H., Jones, C. T., Li, W. K. W., Greenan, B. J. W., Shadwick, E. H., and Burt, W. J. The effect of seasonality in phytoplankton community composition on CO_2 uptake on the Scotian Shelf, Journal of Marine Systems, 147, 52-60, doi:10.1016/j.jmarsys.2014.07.006, 2015.

Crameri, F.: Scientific colour-maps, Zenodo, doi:10.5281/zenodo.1243862, 2018.

380 Dee, D.P., Uppala S., Simmons, A., Berrisford, P., Poli, P., Kobayashi, S., Andrae, U., Balmaseda, M., Balsamo, G., Bauer, d.P., et al.: The ERA-Interim reanalysis: Configuration and performance of the data assimilation system, Quarterly Journal of the Royal Meteorological Society, 137, 553-597, 2011.

Dever, M., Hebert, D., Greenan, B., Sheng, J., and Smith, P.: Hydrography and coastal circulation along the Halifax Line and the connections with the Gulf of St. Lawrence, Atmosphere-Ocean, 54(3), 199-217, doi:10.1080/07055900.2016.1189397,

385 2016.

Doney, S. C.: The growing human footprint on coastal and open ocean biogeochemistry, Science, 328(5985), 1512-1516, doi: 10.1126/science.1185198, 2010.

Egbert, G. D., and Erofeeva, S. Y.: Efficient inverse modeling of barotropic ocean tides, Journal of Atmospheric and Oceanic Technology, 19(2), 183-204, doi: 10.1175/1520-0426(2002)019, 2002.

390 Environment and Climate Change Canada: Canadian Greenhouse Gas Measurement Program, [online] Available from: https://www.canada.ca/en/environment-climate-change/services/climate-change/science-research-data/greenhouse-gases-aerosols-monitoring/canadian-greenhouse-gas-measurement-program.html, 2017.

Evans, W., Hales, B., Strutton, P. G., Shearman, R. K., and Barth, J. A.: Failure to bloom: Intense upwelling results in negligible phytoplankton response and prolonged CO_2 outgassing over the Oregon Shelf, Journal of Geophysical Research:

395 Oceans, 120(3), 1446-1461, doi:10.1002/2014JC010580, 2015.

Fennel, K., Alin, S., Barbero, L., Evans, W., Bourgeois, T., Cooley, S., Dunne, J., Feely, R. A, Hernandez-Ayon, J. M., Hu, X., et al.: Carbon cycling in the North American coastal ocean: A synthesis. Biogeosciences, 16(6), 1281-1304, doi:10.5194/bg-16-1281-2019, 2019.

Fennel, K., and Wilkin, J.: Quantifying biological carbon export for the northwest North Atlantic continental shelves,

400 Geophysical Research Letters, 36 (18), L18605, doi: 10.1029/2009GL039818, 2009.

Fennel, K., Wilkin, J., Levin, J., Moisan, J., O'Reilly, J., and Haidvogel, D.: Nitrogen cycling in the Middle Atlantic Bight: Results from a three-dimensional model and implications for the North Atlantic nitrogen budget, Global Biogeochemical Cycles, 20(3), doi:10.1029/2005GB002456, 2006.

Fiechter, J., Curchitser, E. N., Edwards, C. A., Chai, F., Goebel, N. L., and Chavez, F. P.: Air-sea CO_2 fluxes in the California

405 Current: Impacts of model resolution and coastal topography, Global Biogeochemical Cycles, 28 (4), 371-385, doi:10.1002/2013GB004683, 2014.

Fournier, R. O., Marra, J., Bohrer, R., and Det, M. V.: Plankton dynamics and nutrient enrichment of the Scotian Shelf, Journal of the Fisheries Board of Canada, doi: 10.1139/f77-153, 2011.

Fratantoni, P. S., and Pickart, R. S.: The western North Atlantic shelfbreak current system in summer, Journal of Physical

410 Oceanography, 37(10), 2509-2533, doi:10.1175/JPO3123.1, 2007.

Geshelin, Y., Sheng, J., and Greatbatch, R. J.: Monthly mean climatologies of temperature and salinity in the western North Atlantic, Technical Report, Canadian Data Report of Hydrography and Ocean Sciences, 153, Fisheries and Oceans Canada, 1999.

Gruber, N.: Carbon at the coastal interface. Nature, 517(7533), 148-149, doi:10.1038/nature14082, 2015.

415   Gruber, N., Clement, D., Carter, B. R., Feely, R. A., Van Heuven, S., Hoppema, M., Ishii, M., Key, R. M., Kozyr, A., Lauvset, S. K., et al.: The oceanic sink for anthropogenic CO_2 from 1994 to 2007, Science, 363(6432), 1193-1199, doi:10.1126/science.aau5153, 2019.

Haidvogel, D. B., Arango, H., Budgell, W. P., Cornuelle, B. D., Curchitser, E., Di Lorenzo, E., Fennel, K., Geyer, W. R., Hermann, A. J., Lanerolle, L., et al.: Ocean forecasting in terrain-following coordinates: Formulation and skill assessment of

420   the Regional Ocean Modeling System, Journal of Computational Physics, 227(7), 3595-3624, doi:10.1016/j.jcp.2007.06.016, 2008.

Hannah, C. G., Shore, J. A., Loder, J. W., and Naimie, C. E.: Seasonal circulation on the western and central Scotian Shelf, Journal of Physical Oceanography, 31(2), 591-615, doi:10.1175/1520-0485(2001)031,0591:SCOTWA>2.0.CO;2, 2001.

Hickey, B. M.: Coastal oceanography of western North America from the tip of Baja California to Vancouver Island, in: The

425   Global Coastal Ocean: Regional Studies and Syntheses, volume 11, pp 345-393, Wiley & Sons, New York, 1998.

Ho, D. T., Law, C. S., Smith, M. J., Schlosser, P., Harvey, M., and Hill, P.: Measurements of air-sea gas exchange at high wind speeds in the Southern Ocean: Implications for global parameterizations, Geophysical Research Letters, 33(16), L16611, doi: 10.1029/2006GL026817, 2006.

Kuhn, A.M.: Integration of observations and models for an improved understanding of marine ecosystem dynamics, Dalhousie

430   University. [online] Available from: http://hdl.handle.net/10222/73354, 2017.

Landschützer, P., Gruber, N., Bakker, D. C. E., and Schuster, U.: Recent variability of the global ocean carbon sink, Global Biogeochemical Cycles, 28(9), 927-949, doi:10.1002/2014GB004853, 2014.

Laruelle, G. G., Durr, H. H., Slomp, C. P., and Borges, A. V.: Evaluation of sinks and sources of CO_2 in the global coastal ocean using a spatially explicit typology of estuaries and continental shelves, Geophysical Research Letters, 37(15),

435   doi:10.1029/2010GL043691, 2010.

Laruelle, G. G., Landschützer, P., Gruber, N., Tison, J.-L., Delille, B., and Regnier, P.: Global high-resolution monthly pCO2 climatology for the coastal ocean derived from neural network interpolation, Biogeosciences, 14, 4545-4561, doi:10.5194/bg-14-4545-2017, 2017.

Laruelle, G. G., Lauerwald, R., Pfeil, B., and Regnier, P.: Regionalized global budget of the CO_2 exchange at the air-water

440   interface in continental shelf seas, Global Biogeochemical Cycles, 28(11), 1199-1214, doi:10.1002/2014GB004832, 2014.

Laruelle, G. G., Lauerwald, R., Rotschi, J., Raymond, P. A., Hartmann, J., and Regnier, P.: Seasonal response of air-water CO_2 exchange along the land-ocean aquatic continuum of the northeast North American coast, Biogeosciences, 12(5), 1447-1458, doi:10.5194/bg-12-1447-2015, 2015.

Laurent, A., Fennel, K., Cai, W.-J., Huang, W.-J., Barbero, L., and Wanninkhof, R.: Eutrophication-induced acidification of

445   coastal waters in the northern Gulf of Mexico: Insights into origin and processes from a coupled physical-biogeochemical

model, Geophysical Research Letters, 44, 946-956, doi:10.1002/2016GL071881, 2017.

Laurent, A., Fennel, K., and Kuhn, A.: An observation-based evaluation and ranking of historical earth system model

simulations for regional downscaling in the northwest North Atlantic ocean, Biogeosciences Discussions, doi: 10.5194/bg-

2020-265, 2020.

450   Le Quéré, C., Andrew, R. M., Friedlingstein, P., Sitch, S., Pongratz, J., Manning, A. C., Korsbakken, J. I., Peters, G. P.,

Canadell, J. G., Jackson, R. B., et al.; Global carbon budget 2017, Earth System Science Data, 10(1), 405-448, doi:

10.5194/essd-10-405-2018, 2018.

Lemay, J., Thomas, H., Craig, S. E., Burt, W. J., Fennel, K., and Greenan, B. J.: Hurricane Arthur and its effect on the short-

term variability of pCO_2 on the Scotian Shelf, NW Atlantic, Biogeosciences, 15(7), 2111-2123,doi:10.5194/bg-15-2111-2018,

455   2018.

Loder, J. W., Han, G., Hannah, C. G., Greenberg, D. A., and Smith, P. C.: Hydrography and baroclinic circulation in the

Scotian Shelf region: winter versus summer, Canadian Journal of Fisheries and Aquatic Sciences, 54 (S1), 40-56, doi:

10.1139/f96-153, 1997.

Loder, J. W., Petrie, B., and Gawarkiewicz, G.: The coastal ocean northeastern North America: A large-scale view, in The

460   Sea, Volume 11: The Global Coastal Ocean - Regional Studies and Syntheses, edited by Allan R. Robinson and Kenneth H.

Brink, chap. 5, pp 105-133, John Wiley & Sons, 1998.

Mehrbach, C., Culberson, C. H., Hawley, J. E., and Pytkowicx, R. M.: Measurement of the apparent dissociation constants of

carbonic acid in seawater at atmospheric pressure, Limnology and Oceanography, 18(6), 897-907, doi:

doi:10.4319/lo.1973.18.6.0897, 1973.

465   Millero, F. J.: Thermodynamics of the carbon dioxide system in the oceans, Geochimica et Cosmochimica Acta, 59(4), 661-

677, doi:10.1016/0016-7037(94)00354-O, 1995.

Mills, E. L., and Fournier, R. O.: Fish production and the marine ecosystems of the Scotian Shelf, eastern Canada, Marine

Biology, 54(2), 101-108, doi: 10.1007/BF00386589, 1979.

Petrie, B., Topliss, B. J., and Wright, D. G.: Coastal upwelling and eddy development off Nova Scotia, Journal of Geophysical

470   Research: Oceans, 92 (C12), 12979-12991, doi:10.1029/JC092iC12p12979, 1987.

Previdi, M., Fennel, K., Wilkin, J., and Haidvogel, D.: Interannual variability in atmospheric CO_2 uptake on the northeast U.S.

continental shelf, Journal of Geophysical Research, 114(G4), G04003, doi:10.1029/2008JG000881, 2009.

Rodenbeck, C., Bakker, D. C. E., Gruber, N., Iida, Y., Jacobson, A. R., Jones, S., Landschützer, P., Metzl, N., Nakaoka, S.,

Olsen, A., et al.: Data-based estimates of the ocean carbon sink variability: First results of the Surface Ocean pCO_2 Mapping

475   intercomparison (SOCOM), Biogeosciences, 12(23), 7251-7278, doi: 10.5194/bg-12-7251-2015, 2015.

Roobaert, A., Laruelle, G. G., Landschützer, P., Gruber, N., Chou, L., and Regnier, P.: The spatiotemporal dynamics of the sources and sinks of CO_2 in the global coastal ocean, Global Biogeochemical Cycles, 33(12), 1693-1714, doi: 10.1029/2019GB006239, 2019.

480 Ross, T., Craig, S. E., Comeau, A., Davis, R., Dever, M., and Beck, M.: Blooms and subsurface phytoplankton layers on the Scotian Shelf: Insights from profiling gliders, Journal of Marine Systems, 172, 118-127, doi:10.1016/j.jmarsys.2017.03.007, 2017.

Rutherford, K., and Fennel, K.: Diagnosing transit times on the northwestern North Atlantic continental shelf, Ocean Science, 14(5),1207-1221, doi: 10.5194/os-14-1207-2018, 2018.

Seitzinger, S. P., Harrison, J. A., Dumont, E., Beusen, A. H. W., and Bouwman, A. F.: Sources and delivery of carbon, nitrogen,
485 and phosphorus to the coastal zone: An overview of Global Nutrient Export from Watersheds (NEWS) models and their application, Global Biogeochemical Cycles, 19(4), doi: 10.1029/2005GB002606, 2005.

Shadwick, E. H. and Thomas, H.: Seasonal and spatial variability in the CO_2 system on the Scotian Shelf (northwest Atlantic), Marine Chemistry, 160, 42-55, doi:10.1016/j.marchem.2014.01.009, 2014.

Shadwick, E., Thomas, H., Azetsu-Scott, K., Greenan, B., Head, E., and Horne, E.: Seasonal variability of dissolved inorganic
490 carbon and surface water pCO_2 in the Scotian Shelf region of the northwestern Atlantic, Marine Chemistry, 124(1-4), 23-37, doi: 10.1016/j.marchem.2010.11.004, 2011.

Shadwick, E. H., Thomas, H., Comeau, A., Craig, S. E., Hunt, C. W., and Salisbury, J. E.: Air-sea CO_2 fluxes on the Scotian Shelf: Seasonal to multi-annual variability, Biogeosciences, 7(11), 3851-3867, doi: 10.5194/bg-7-3851-2010, 2010.

Shan, S., Sheng, J., and Greenan, B. J.. Physical processes affecting circulation and hydrography in the Sable Gully of Nova
495 Scotia, Deep Sea Re-search Part II: Topical Studies in Oceanography, 104, 35-50, doi:10.1016/j.dsr2.2013.06.019, 2014.

Shan, S., Sheng, J., Ohashi, K., and Dever, M.. Assessing the performance of a multi-nested ocean circulation model using satellite remote sensing and in-situ observations, Satellite Oceanography and Meteorology, 1(1), 39-59, doi:10.18063/SOM.2016.01.004, 2016.

Signorini, S. R., Mannino, A., Najjar Jr, R. G., Friedrichs, M. A., Cai, W.-J., Salisbury, J., Wang, Z. A., Thomas, H., and
500 Shadwick, E.: Surface ocean pCO_2 seasonality and sea-air CO_2 flux estimates for the North American east coast, Journal of Geophysical Research: Oceans, 118(10), 5439-5460, doi:10.1002/jgrc.20369, 2013.

Takahashi, T., Sutherland, S. C., Sweeney, C., Poisson, A., Metzl, N., Tilbrook, B., Bates, N., Wanninkhof, R., Feely, R. A., Sabine, C., Olafsson, J., and Nojiri, Y.: Global sea air CO_2 flux based on climatological surface ocean pCO_2, and seasonal biological and temperature effects, Deep Sea Re-search Part II: Topical Studies in Oceanography, 49(9), 1601-1622, doi:
505 10.1016/S0967-0645(02)00003-6, 2002.

Tsunogai, S., Watanabe, S., and Tetsuro, S.: Is there a "continental shelf pump" for the absorption of atmospheric CO_2? Tellus, (51B), 701-712, doi:10.1034/j.1600-0889.1999.t01-2-00010.x, 1999.

Turi, G., Lachkar, Z., and Gruber, N.: Spatiotemporal variability and drivers of pCO_2 and air-sea CO_2 fluxes in the California Current system: An eddy-resolving modeling study, Biogeosciences, 11(3), 671-690, doi:10.5194/bg-11-671-2014, 2014.

510   Umlauf, L., and Burchard, H.: A generic length-scale equation for geophysical turbulence models, Journal of Marine Research, 61(2), 235-265, doi:10.1357/002224003322005087, 2003.

Urrego-Blanco, J., and Sheng, J.: Interannual variability of the circulation over the Eastern Canadian shelf, Atmosphere-Ocean, 50(3), 277-300, doi:10.1080/07055900.2012.690430, 2012.

Vandemark, D., Salisbury, J. E., Hunt, C. W., Shellito, S. M., Irish, J.D., McGillis, W. R., Sabine, C. L., and Maenner, S. M.:

515   Temporal and spatial dynamics of CO_2 air-sea flux in the Gulf of Maine, Journal of Geophysical Research: Oceans, 116 (C1), C01012, doi:10.1029/2010JC006408, 2011.

Warner, J. C., Sherwood, C. R., Arango, H. G., and Signell, R. P.: Performance of four turbulence closure models implemented using a generic length scale method, Ocean Modelling, 8(1), 81-113, doi: 10.1016/j.ocemod.2003.12.003, 2005.

Weiss, R.F.: Carbon dioxide in water and seawater: The solubility of a non-ideal gas, Marine Chemistry, 2(3), 203-215, 1974.

520   Wu, H. and Zhu, J.: Advection scheme with 3rd High-order Spatial Interpolation at the Middle Temporal level and its application to saltwater intrusion in the Changjiang Estuary, Ocean Modelling, 33(1-2), 33-51, doi:10.1016/j.ocemod.2009.12.001, 2010.

Xiu, P., Chai, F., Curchitser, E. N., and Castruccio, F. S.: Future changes in coastal upwelling ecosystems with global warming: The case of the California Current System, Scientific Reports, 8(1), 2866, eoi:10.1038/s41598-018-21247-7, 2018.

525   Zeebe, R. E., and Wolf-Gladrow, D. A.: CO_2 in Seawater: Equilibrium, Kinetics, Isotopes, 1st Ed. Amsterdam: Elsevier Science B.V., 2001.
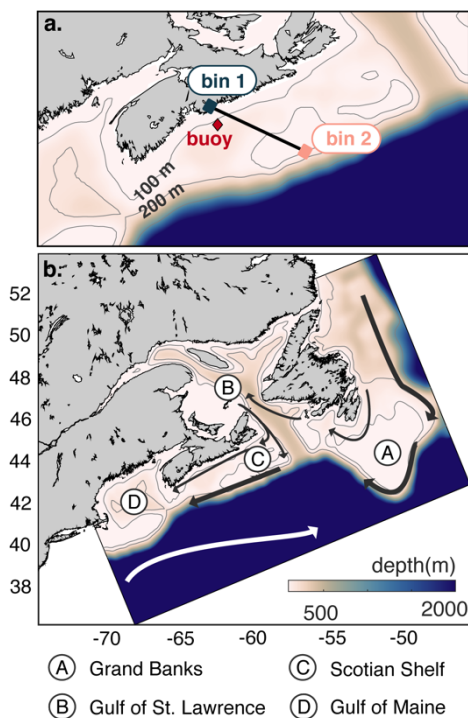
Figure 1: Bathymetric maps of the model domain. Bottom panel shows the model domain with mean current locations. Top panel
530   **zooms in on the Scotian Shelf, and indicates the location of the CARIOCA buoy (red diamond) and the Atlantic Condor Transect (black line). Both maps show the 100 m and 200 m isobaths.**
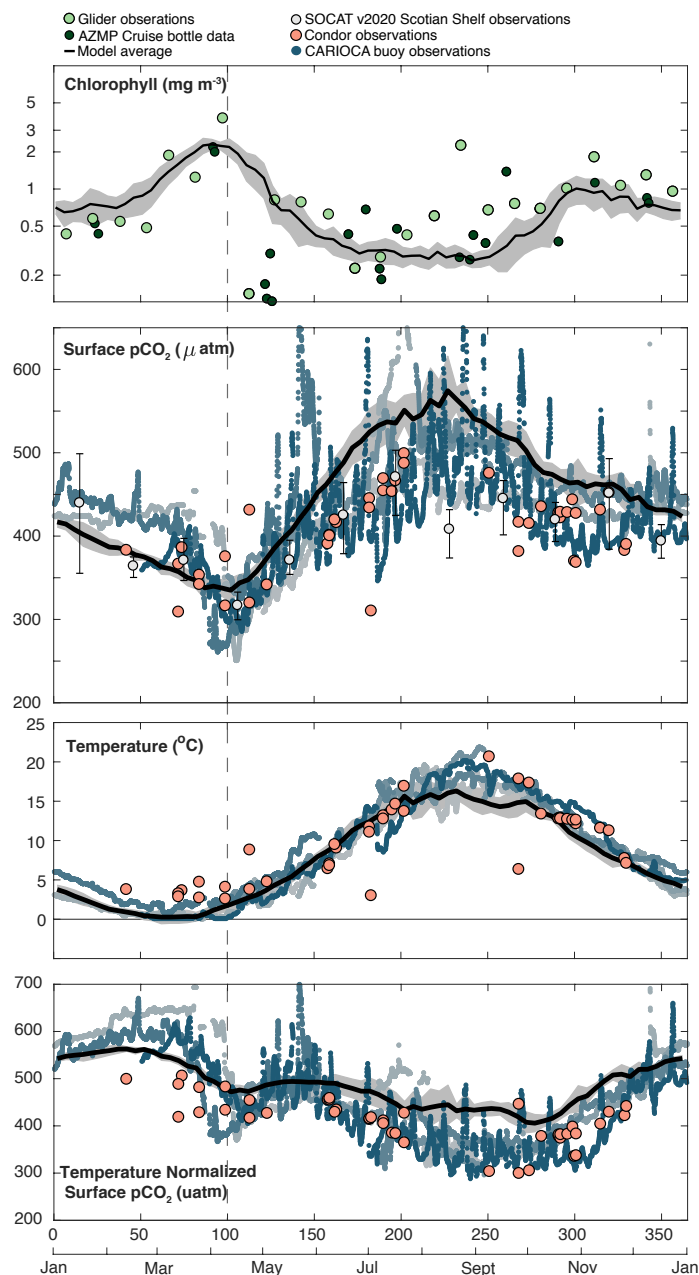
Figure 2: Seasonal (from top to bottom) (a) chlorophyll (Glider: RMSE: 0.46, bias: -0.007; AZMP: RMSE: 0.67, bias: 0.18); (b)
pCO₂ (RMSE: 58.1, bias: -21.3); (c) temperature (RMSE: 1.8, bias: 0.8); (d) temperature normalized pCO₂ (RMSE: 63.6, bias: -
535 **29.5) at STN 2 on the Scotian Shelf. The model mean is shown with the thick black line and standard deviation with the grey**
shaded area in all panels. In (a) the dark green points are AZMP bottle data and light green points are glider data. In (b-d)
observations from the moored CARIOCA buoy are shown as small blue points and observations from the Atlantic Condor
transects at approximately the same location as the buoy are shown in large pink points. Light grey points are monthly mean
SOCAT observations for the entire Scotian Shelf and the error bars are the 10ᵗʰ and 90ᵗʰ percentiles.
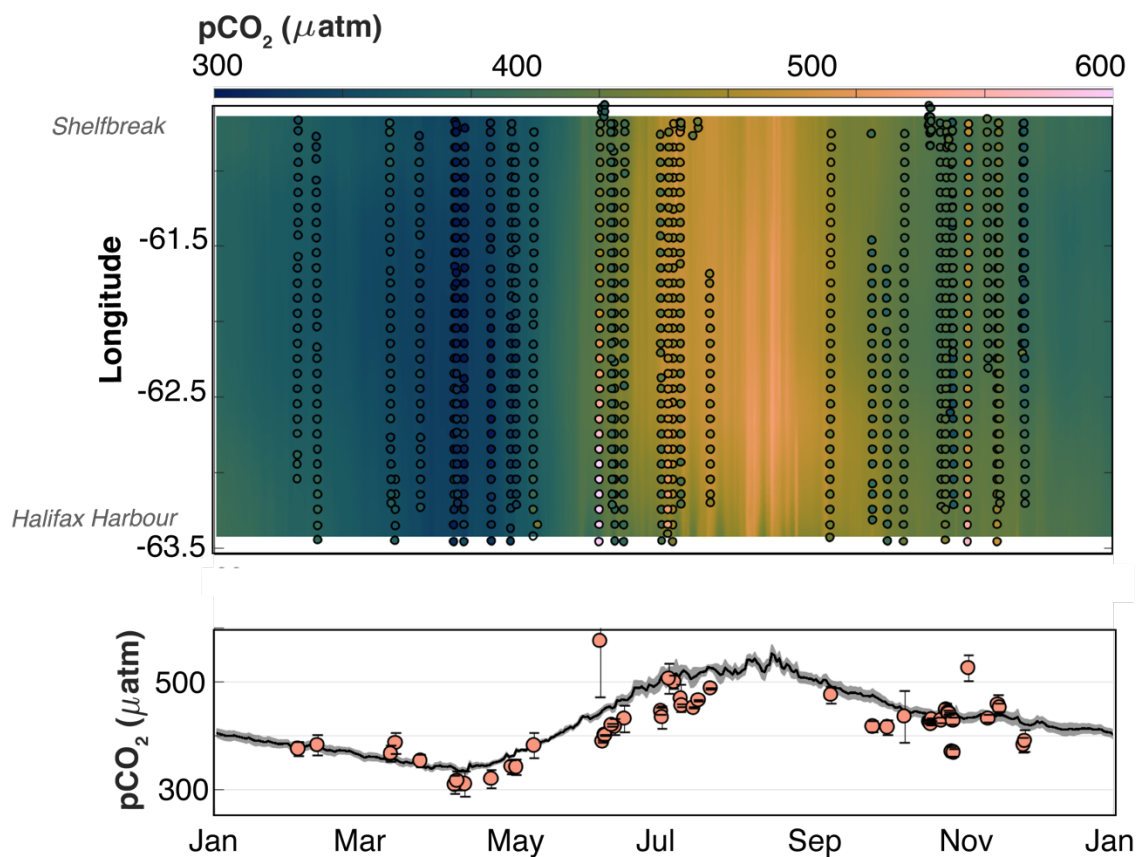
540

Figure 3: Model-data comparison along the Atlantic Condor transect. The top panel shows pCO_2 (in colour) evolving over time (x-axis) along the transect (longitude on the y-axis; Halifax Harbour to Shelfbreak). The background is the model average pCO_2 along the transect and the points are the Atlantic Condor data binned into 0.1° longitudinal bins. The bottom panel shows the average pCO_2 along the transect (y-axis) as it evolves over the seasonal cycle (x-axis). The line and shaded area are the model mean

545 **and standard deviation, respectively, both across the transect and across the 5 years of simulations. The points are the average and the error bars are standard deviation of observational pCO_2 across each transect. *RMSE: 20.3 μatm; Bias: 4.1 μatm***
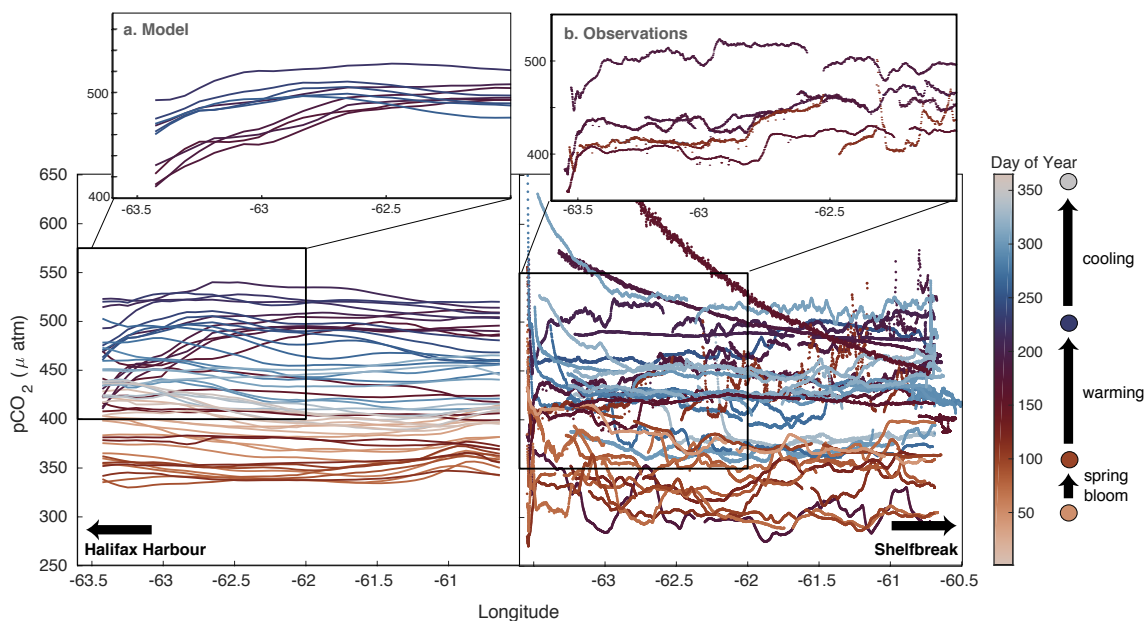
Figure 4: Temporal evolution of *p*CO₂ across the Atlantic Condor transect. X-axis is longitude, with the Halifax Harbour indicated on the left-hand side and the Shelfbreak indicated on the right-hand side of each panel; Y-axis is *p*CO₂; and the colour indicates the day of the year. The left panel is year 2000 of the model along the transect every 5 days. The right panel are the observations along the transect.

550
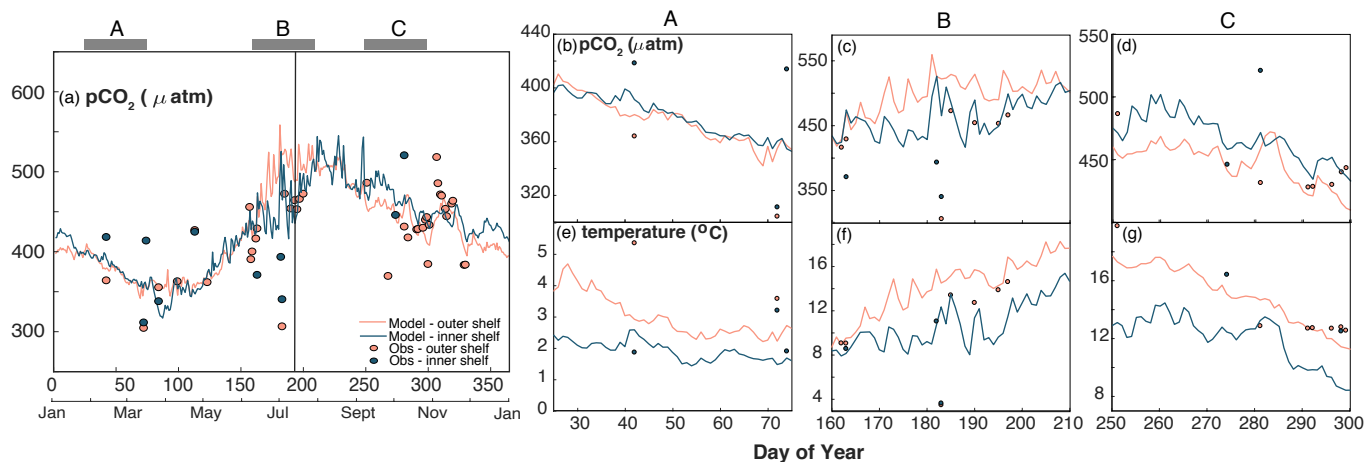
Figure 5: Comparison of nearshore with offshore seasonal cycles of *p*CO₂. Blue indicates the average *p*CO₂ in a 0.5° longitude bin nearshore and pink indicates 0.5° bin near the shelfbreak along the Atlantic Condor transect (Figure 1). The lines indicate model output and points indicate observations from the Atlantic Condor transect. The thick black line in panel (a) indicates time slice for Figure 6. The top panel shows the full seasonal cycle of *p*CO₂ and the lower panels show *p*CO₂ and temperature for specific time slices, that are indicated by the three grey bars (A-C) in the top panel.

555
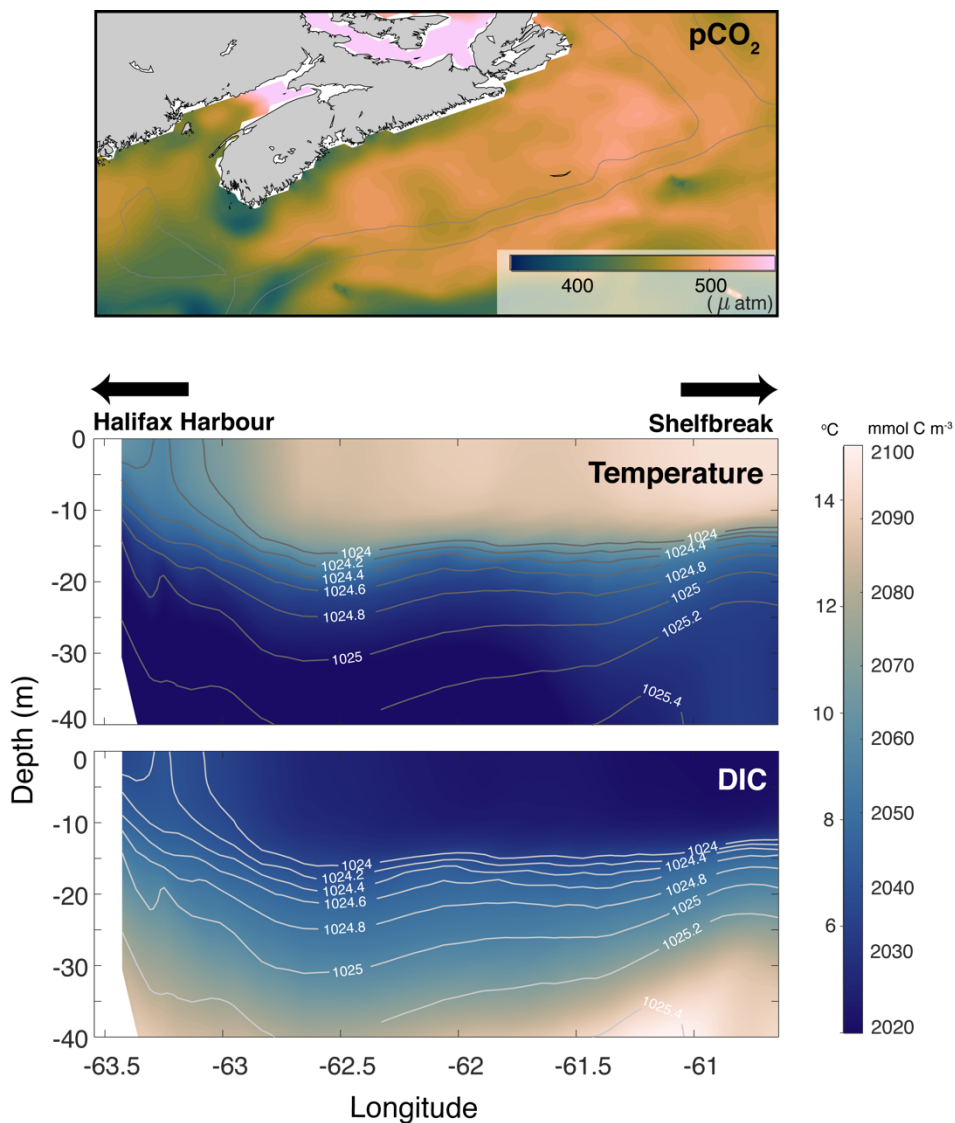
Figure 6: Surface map of *p*CO₂ (top panel), and transects along the average Atlantic Condor ship track of temperature (middle
560 **panel) and DIC (bottom panel) from the model taken during an upwelling event (Jul 11, 2000). Contours in the transects are**
density.
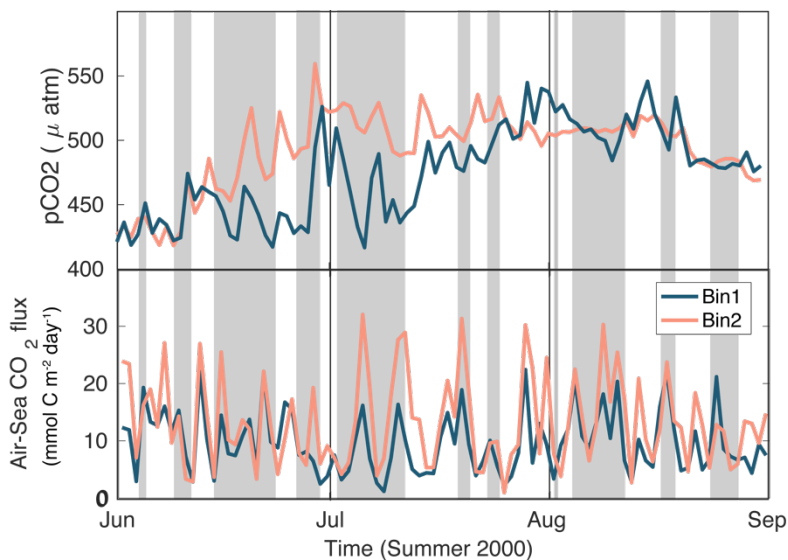
Figure 7: Timeseries of modeled pCO$_2$ (top panel) and air-sea CO$_2$ flux (bottom panel) throughout the summer months of 2000.
565 **Shaded area indicates when there was upwelling-favourable winds nearshore. The blue lines indicate the values from nearshore bin and the pink lines indicate values from the offshore bin (see Figure 1).**
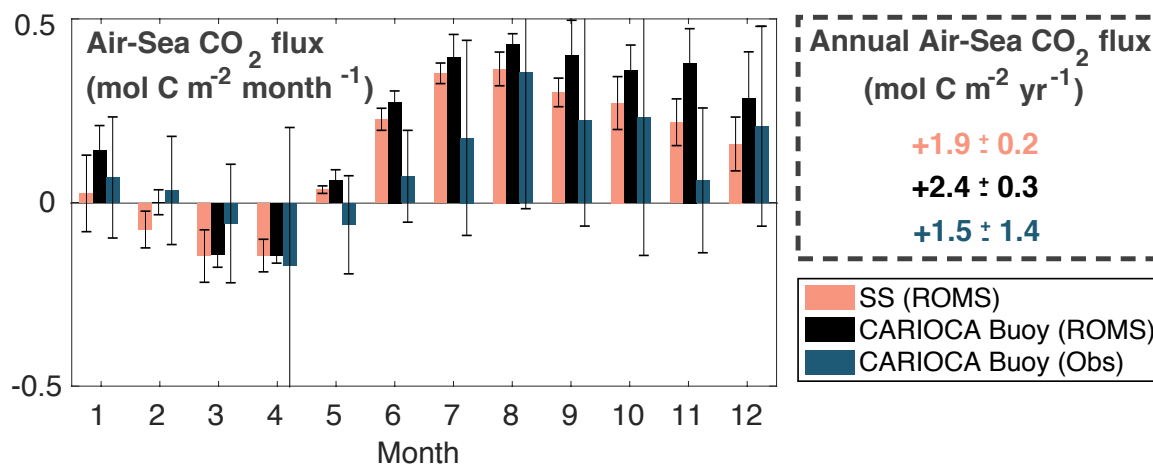
Figure 8: Monthly and annual air-sea CO$_2$ flux calculated from the model on the entire Scotian Shelf (pink), at the CARIOCA buoy location (black), and from the buoy observations (blue).

570
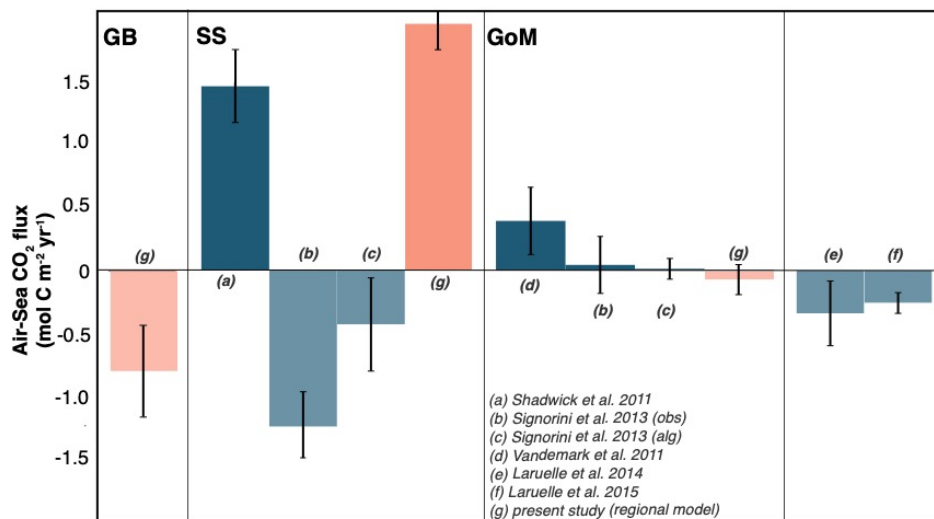
Figure 9: Annually integrated air-sea CO₂ flux for the Grand Banks (GB), Scotian Shelf (SS) and Gulf of Maine (GoM) in the model (pink) compared to literature values (blue). Positive values are net outgassing and negative values are net ingassing.
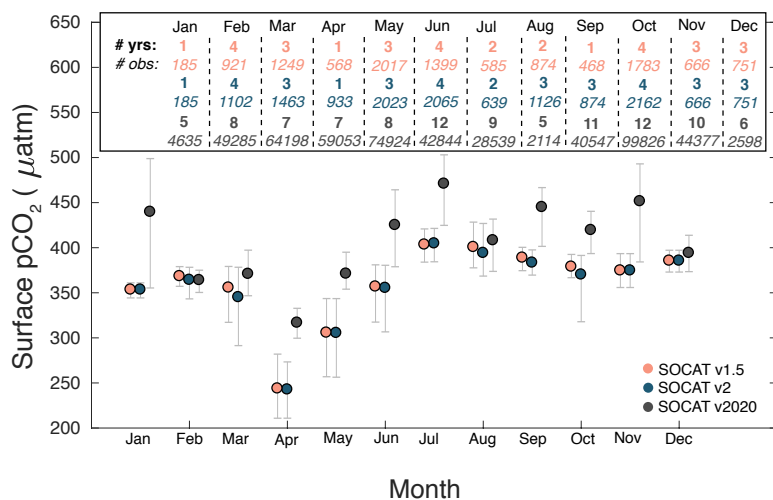
575 **Figure 10: Comparison of the seasonal cycle of pCO$_2$ for the different versions of SOCAT for the Scotian Shelf. The points indicate the mean for each month and the bars indicate the 5th and 95th percentile. Inset shows the number of years and number of observations used in each month for each version.**